

Stability Analyses of Delay Differential Equations in Climate Modeling

Alan Chen, Ayushman Choudhury

APMA2190 Final Project
December 2024

Contents

1	Introduction	1
2	Energy Balance Temperature Model with Time Delayed Albedo Effect	2
2.1	Interlude: Exponential Perturbation Stability Analysis	3
2.2	Stability Analysis of Eq. 2	5
2.3	Numerical Solution	7
3	Models of El Niño Southern Oscillation	7
3.1	History of models	9
3.2	Stability Analysis of Eq. 19	9
3.3	Numerical Analysis of Eq. 21	12
4	Concluding thoughts	13

1 Introduction

In their simplest form, ordinary differential equations (ODEs) are Markovian in some sense - future changes depend strictly on the instantaneous current state of the system. However, in climate modeling, this is unrealistic; physical systems possess past dependencies and different components influence each other with delayed feedback loops. Naturally, ODEs can be extended to a new class of **delay differential equations** (DDEs) that simply allow the change in state to depend on the system state at previous moments in time:

$$\dot{u}(t) = f(u(t), u(t - \tau_1), u(t - \tau_2), \dots, u(t - \tau_m)), \tag{1}$$

where $u \in \mathbb{R}^n$ and each of τ_i for $i = 1, 2, \dots, m$ represents a specific **time-delay effect** or **feedback loop** [5].

Clearly, time delay effects are much more realistic compared to the simple instantaneous ODEs, especially in climate systems. As a simple example, the albedo (fraction of solar radiation reflected by Earth's surface) of Earth has significant implications for temperature regulation. However,

Earth’s systems are robust and have significant “temperature inertia” i.e. changes in energy take time before converting into measurable temperature changes, so an accurate model would need to account for the delay of albedo impact on the change on temperature.

We present a few case studies of DDEs used in climate modeling. In section 2, we walk through a very coarse zero-dimensional temperature example model with a time delayed albedo effect, along with providing novel numerical perspectives that provide visual intuition to the types of unique dynamics that can emerge in DDEs, including a stability analysis of the equilibria and numerical solutions for various values of the time delay that uncover a supercritical Hopf bifurcation. In section 3, we switch gears to models of specific climate systems, in particular the El Niño Southern Oscillation (ENSO). We discuss a brief history of how modeling ENSO has changed over the years and again study the steady states and their respective stabilities in fundamental models. We also visualize numerical solutions. Throughout the report, we rely heavily on visual and numerical intuition and keep the calculations light as the theoretical grunt work has already been outlined in the literature.

2 Energy Balance Temperature Model with Time Delayed Albedo Effect

In [1], Andersson and Lundberg propose a **zero-dimensional**¹ energy balance effect model of globally averaged temperature $T : \mathbb{R} \rightarrow \mathbb{R}$ (in Kelvins). In particular, they consider a compartment-esque model with a time-delayed albedo term that impacts the absorbed energy:

$$C_1 \dot{T} = \underbrace{Q_0(1 - \alpha(T(t - \tau)))}_{\text{incoming absorbed energy}} - \underbrace{\sigma g(T)T^4}_{\text{outgoing emitted energy}}, \quad (2)$$

where $C_1 > 0$, Q_0 , σ , and g are the globally averaged heat capacity, mean solar radiative input, Boltzmann constant, and the effective emissivity coefficient as a function of T , respectively. The albedo effect, α , is defined piecewise as

$$\alpha(T) = \begin{cases} 0.85 & T \leq 216 \\ 2.798 - 0.009T & 216 < T < 283 - B \\ 2.798 - 0.009T + A \left(1 - \cos\left(\frac{2\pi(T-283-B)}{B}\right)\right) & 283 - B \leq T < 283 \\ 0.25 & 283 \leq T \end{cases} \quad (3)$$

and $g(T) = 1 - m \tanh((T/T_0)^6)$ where $m = 0.5$ and $T_0 = 284.15$ K. We refer readers interested in discussion of the explicit values of the other constants, their derivations, and overall physical motivation of the terms to [1]. The particular motivation for the albedo delay is simple: the model can now account for the imbalance between the slow buildup yet fast melting of ice volume and the empirically observed delay between global temperature changes and ice volume.²

The beauty of this system is its simplicity (it is really only one dimension!) that nevertheless yields interesting dynamics once we permit $\tau > 0$. Before we dive into the analysis, we review a method of stability analysis for ODEs in order to extend it to DDEs.

¹“zero-dimensional” refers to zero spatial dimensions.

²It is estimated the true delay is between 10^3 and 10^4 years.

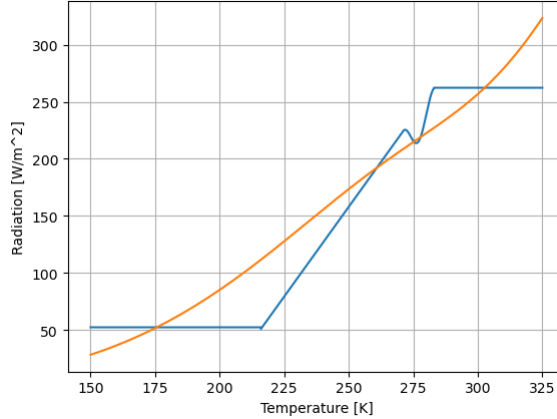


Figure 1: (Replication of figure 1 in [1]): Comparison of incoming absorbed energy term (blue) and outgoing emitted energy term (orange) for various values of T (both are evaluated at the same T). We note 5 equilibria (where $\dot{T} = 0$).

2.1 Interlude: Exponential Perturbation Stability Analysis

Consider the ODE system

$$\dot{u} = f(u), u \in \mathbb{R}^n. \quad (4)$$

Our general approach to analyzing the stability of equilibria in eq. 4 has been to

1. find the equilibria by solving $f(u) = 0$,
2. linearize the system around equilibria points u^* ,
3. and look at the sign on the real part of the eigenvalues of the Jacobian matrix.

Unfortunately, extending this approach to DDEs is not clear because of the additional delay term. Instead, we present an analogous approach to analyze stability of equilibria that is equivalent in the finite dimensional case but extends itself more easily to the DDE case.

Intuitively, we will analyze *small exponential perturbations around equilibrium points*. Let u^* be an equilibrium of eq. 4 and consider a solution of the form

$$u(t) = u^* + v(t) \quad (5)$$

where $\|v(t)\| \ll 1$ models a small perturbation around the equilibrium u^* . Then, through substitution into a linearized form of eq. 4, we find that

$$\dot{v}(t) = \mathcal{J}_f(u^*)v, \quad (6)$$

where $\mathcal{J}_f(u^*)$ is the Jacobian of f evaluated at u^* . This results in v taking the form $v(t) = v_0 e^{\lambda t}$, where v_0 is an eigenvector of $\mathcal{J}_f(u^*)$ and λ is the corresponding eigenvalue. Then, we can analyze the limiting behavior of v based on the sign of the real component in λ , which we observe recovers *exactly* the original finite-dimensional approach.

However, this perturbation perspective extends much more directly to analyzing eq. 1. First, we naturally define the equilibria of the system by finding u^* such that

$$f(\underbrace{u^*, u^*, \dots, u^*}_{m \text{ times}}) = 0. \quad (7)$$

This essentially is assuming that the initial “window” of the solution is all constant at u^* . For clarity, we now only consider $m = 1$ since 2 only has $m = 1$; the results extend trivially to $m > 1$. Using the same solution as eq. 5, we can find that

$$\dot{v}(t) = Av(t) + Bv(t - \tau) \quad (8)$$

where

$$A = \frac{\partial f}{\partial u_1}(u^*, u^*) \quad (9)$$

$$B = \frac{\partial f}{\partial u_2}(u^*, u^*) \quad (10)$$

are both square $n \times n$ matrices. The same solution form appears as $v(t) = v_0 e^{\lambda t}$. This gives that

$$\frac{d}{dt}(v_0 e^{\lambda t}) = Av_0 e^{\lambda t} + Bv_0 e^{\lambda(t-\tau_1)} \quad (11)$$

$$\lambda v_0 = (A + B e^{-\lambda \tau_1})v_0. \quad (12)$$

Because of the delay, we have now picked up an additional $e^{-\lambda \tau_1}$ term that transforms a simple eigenvalue-eigenvector problem in the finite dimensional case into solving the **characteristic equation**

$$\det(A + B e^{-\lambda \tau_1} - \lambda I) = 0 \quad (13)$$

for λ . In general, this is not possible to solve explicitly. We will see in a moment that even in 1D the characteristic equation is implicit and transcendental. However, the rest of the analysis is identical - because of the nature of v , the real part of λ once again governs the growth rate of the solution.

When $n = 1$, this equation reduces to just

$$a + b e^{-\lambda \tau_1} - \lambda = 0 \quad (14)$$

where a and b are now scalars.

Lemma 1. *Assume $n = 1$. Then, $c = \text{Re}(\lambda)$ and $d = \text{Im}(\lambda)$ solve*

$$c = a + b e^{-c \tau_1} \cos(d \tau_1) \quad (15)$$

$$d = -b e^{-c \tau_1} \sin(d \tau_1). \quad (16)$$

To allow these transcendental equations to be solved stably numerically using the constants at hand, we let $x = c \tau_1$ and $y = d \tau_1$ so that

$$x = a \tau_1 + b \tau_1 e^{-x} \cos(y)$$

$$y = -b \tau_1 e^{-x} \sin(y).$$

Proof. This lemma can be derived strictly from expanding λ as $c + di$ so that $c = \text{Re}(\lambda)$ and $d = \text{Im}(\lambda)$. Substituting for λ in the characteristic equation shows

$$\begin{aligned} a + be^{-c\tau_1 - d\tau_1 i} &= c + di \\ a + be^{-c\tau_1}(\cos(-d\tau_1) + i \sin(-d\tau_1)) &= c + di \end{aligned}$$

so that matching the real coefficients and the imaginary coefficients gives, as desired,

$$\begin{aligned} c &= a + be^{-c\tau_1} \cos(d\tau_1) \\ d &= -be^{-c\tau_1} \sin(d\tau_1) \end{aligned}$$

where we used that \cos is even and \sin is odd to clean up the expression. \square

2.2 Stability Analysis of Eq. 2

In the general $\tau \geq 0$ case, we can numerically find the equilibria of eq. 2 T_i^* for $i = 1, 2, \dots, 5$:

$$T^* = [175.64, 260.82, 274.24, 277.84, 302.69]. \quad (17)$$

Immediately note that when $\tau = 0$, the equilibria and stability are easily visible from figure 1, which plots the incoming absorbed energy and the outgoing emitted energy for various values of T . The intersection points are the equilibria and the stability is governed by the sign of \dot{T} on either side of the equilibria. In particular, we see that T_1^* , T_3^* , and T_5^* are stable while T_2^* and T_4^* are unstable. We use this as a sanity check of our general τ numerical methods.

Returning back to the general system, we can derive the functional forms of a and b from the functional forms of g and α respectively. For an equilibrium T_i^* , using the product rule, chain rule, and a derivatives table, we can find

$$\begin{aligned} a &= -\sigma C_1^{-1} \left(-\frac{3(T_i^*)^9 \cosh^{-2}((T_i^*/T_0)^6)}{T_0^6} + 4(T_i^*)^3 g(T_i^*) \right) \\ b &= -Q_0 C_1^{-1} \alpha'(T_i^*) \end{aligned}$$

where

$$\alpha'(T) = \begin{cases} 0 & T \leq 216 \\ -0.009 & 216 < T < 283 - B \\ -0.009 + \frac{2\pi A}{B} \sin\left(\frac{2\pi(T-283-B)}{B}\right) & 283 - B \leq T < 283 \\ 0 & 283 \leq T \end{cases}.$$

Although there are theoretical stability criteria that can be used to analyze the real part of the solutions (c) to the equations in Lemma 1 (see [4]), we present a purely numerical perspective as visual intuition.

Let $\text{sign} : \mathbb{R} \rightarrow \{-1, 1\}$ denote the sign function that maps all negative reals to -1 and all nonnegative reals to 1 . In fig. 2, we plot $\text{sign}(c)$ for various time delays between 0 and 4×10^{10} seconds. The equilibrium is stable when $\text{sign}(c) = -1$ and unstable when $\text{sign}(c) = 1$.

We observe that T_1^* and T_5^* are unconditionally (on τ) stable and T_2^* and T_4^* are unconditionally (on τ) unstable. However, T_3^* exhibits a *supercritical Hopf bifurcation*, as a periodic orbit emerges as a result of two eigenvalues passing over the imaginary axis at the same time when τ surpasses

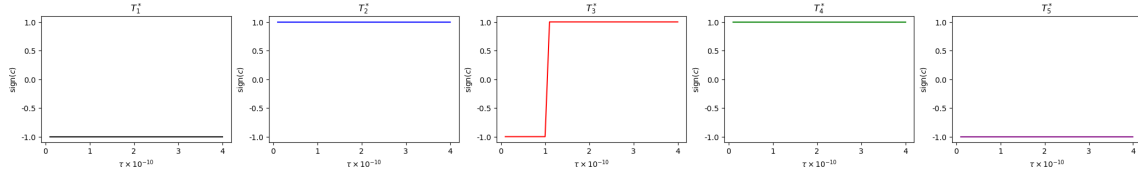


Figure 2: $\text{sign}(\text{Re}(c))$ for various values of τ . Equilibrium 1 and 5 are unconditionally stable for all τ where as equilibrium 2 and 4 are unconditionally unstable. Equilibrium 3 undergoes a bifurcation where it flips from stable to unstable after a critical delay τ_c . The plots are linearly interpolated.

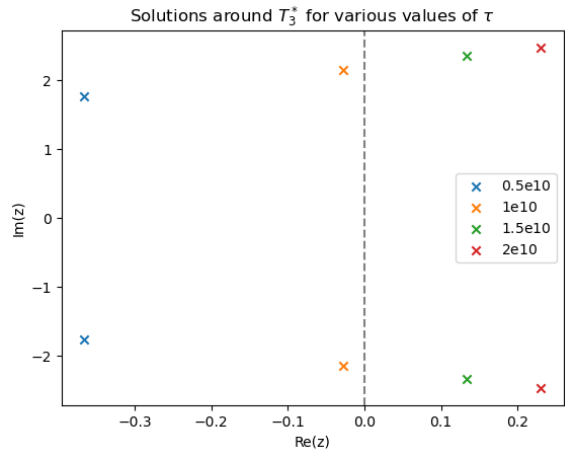


Figure 3: We plot the solutions to the characteristic equation around T_3^* . We can see two roots pass across the imaginary axis simultaneously as τ increases.

a critical value $\tau_c \in [10^{10}, 2 \times 10^{10}]$ (the true value of $\tau_c \approx 1.02 \times 10^{10}$ s or about 325 years.). The bifurcation is supercritical because the equilibrium goes from being stable to unstable.

In other words, there exists a critical delay of the albedo effects around 300 years that transitions the system from stable at T_3^* to unstable - the nature of the bifurcation is clear once visualizing the solutions for various values of τ around T_3^* in fig. 3. It is surprising that interesting structure could emerge in such a simple model.

2.3 Numerical Solution

Following [1], we can numerically solve the equation by mildly adapting the RK4 method to forward step through time while accounting for the new delay term. The RK4 steps are shown below, with the additional delay modification underlined and $h = \tau/ds$ as the step size, where d is some hyperparameter representing the number of discretized steps that are equivalent to a “lookback” of τ s. Letting T_i denote the discretized solution at step i (equivalent of ih seconds),

$$\begin{aligned} k_1 &= f(T_n, \underline{T_{n-d}}) \\ k_2 &= f(T_n + hk_1/2, \underline{T_{n-d}}) \\ k_3 &= f(T_n + hk_2/2, \underline{T_{n-d}}) \\ k_4 &= f(T_n + hk_3, \underline{T_{n-d}}) \\ T_{n+1} &= T_n + \frac{h}{6}(k_1 + 2k_2 + 2k_3 + k_4). \end{aligned}$$

For numerical stability, we generate the solution C_1T before scaling back down to just get T . We specify a constant initial window of size τ and plot the resulting solution for various values of τ in fig. 4. We start all trials at a small perturbation around T_3^* because the other equilibria do not have any interesting behavior.

Once the length of the feedback loop surpasses the critical τ , we observe an unstable periodic orbit bifurcate from an originally asymptotically stable system, as expected from a supercritical Hopf bifurcation. Furthermore, the system continues undergoing a series of period doubling bifurcations as τ increases before becoming essentially chaotic (fig. 5).

The physical significance of T_3^* likely lies in that 274.24 is around 1 degree C, or right above the freezing point of water. If globally averaged temperatures are near this point, it has implications for the water cycle and if ice volume is expanding or shrinking. We have shown that longer delay in the albedo term introduces instability around this point, resulting in periodic oscillations that bounce around but are never that large in magnitude (to where they dip below 0 degrees C). Overall, the physical meaning of this equilibrium offers some vague understanding as to why this steady state exhibits special behavior compared to the unconditional behavior of the others.

3 Models of El Niño Southern Oscillation

We now turn to a different application of DDEs.

One of the most active climate phenomena on Earth is the El Niño Southern Oscillation (hereafter ENSO), which affects the tropical regions of the Pacific Ocean. This oscillation has two phases: El Niño, associated with higher temperatures and precipitation in the East near South America,

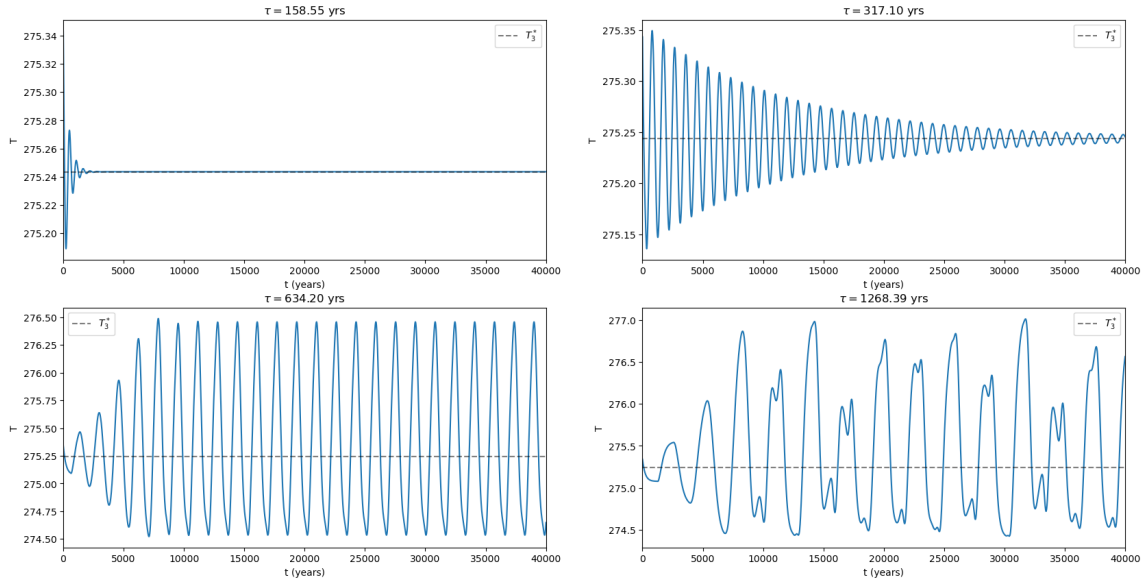


Figure 4: We simulate solutions with initial conditions near T_3^* for various τ . For $\tau \geq \tau_c$, a periodic orbit emerges, and the period lengthens through period doubling bifurcations as τ continues to increase.

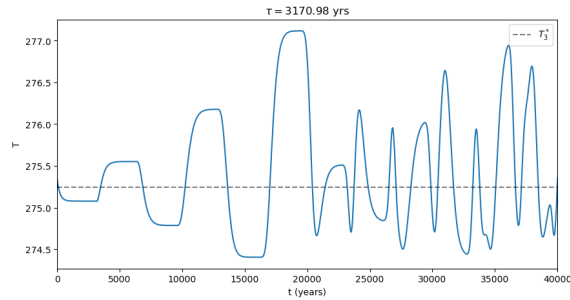


Figure 5: For $\tau = 10^{11}$ seconds, after a cascade of period doubling bifurcations, the dynamics of the zero dimensional system appear to be essentially chaotic.

and La Niña, associated with higher temperatures and precipitation in the West near Australia and South America. These cycles occur ever 2-7 years, but are difficult to predict with precision.

ENSO is primarily driven by the Bjerknes feedback, where a warming of the Eastern Pacific waters weakens the strength of the east-to-west trade winds in the atmosphere, which slows the upwelling of cold water from the depths of the Eastern Pacific ocean, which keeps the surface waters warm, and so on, causing the strong El Niño effect.

Bjerknes proposed this feedback in 1969 [2], and is considered to be a founding figure in the study of ENSO dynamics.

3.1 History of models

Twenty years following Bjerknes' groundbreaking paper, Suarez and Schopf [6] proposed a mechanism to limit Bjerknes' positive feedback loop, ensuring that eventually the ocean state returns to equilibrium. Specifically considering the Sea Surface Temperature (hereafter SST) anomalies, they started with the simple Ordinary Differential Equation:

$$\dot{T} = \underbrace{kT}_{\text{SST anomaly growth}} - \underbrace{bT^3}_{\text{nonlinear effects on SST anomaly}} \quad (18)$$

This can be simplified by scaling time by k^{-1} and T by $(k/b)^{1/2}$ to remove the coefficients.

Suarez and Schopf's argument claimed that Rossby waves propagated on the ocean thermocline from the warming region in the east, towards the western boundary, and then reflected back towards the east as Kelvin waves, cooling the basin back to normal once they arrived. In this process, the "signal" of the SST anomaly was reentered after some time delay for these waves to cross the Pacific Ocean and return. Thus, describing this mechanism necessitated a Delay Differential Equation:

$$\dot{T} = \underbrace{T - T^3}_{\text{scaled ODE}} - \underbrace{\alpha T(t - \tau)}_{\text{delay term}} \quad (19)$$

Five years later, Tziperman et al. [7] expanded on eq. 19 in several ways. First, they quantified the delay by the speeds of the Rossby Wave and Kelvin Wave (C_R and C_K), and the width of the basin, i.e. the length the waves must travel before being reflected (L). Second, they wrote their equation in terms of the Thermocline Depth anomaly $h(t)$ instead, which is still closely related to the SST anomaly. Third, they added an idealized seasonal forcing, with frequency ω_a . Combining these modifications leaves a complicated DDE:

$$\dot{h}(t) = \alpha A \left(h \left\{ t - \left[\frac{L}{2C_K} \right] \right\} \right) - \beta A \left(h \left\{ t - \left[\frac{L}{C_K} + \frac{L}{2C_R} \right] \right\} \right) + \gamma \cos(\omega_a(t)). \quad (20)$$

In 2008, Ghil et al. [3] considered the dynamics of a simplified version of 20. They condensed the two-delay model to one delay τ , and defined $A(x) = \tanh(x)$, resulting in the cleaner

$$\dot{h}(t) = \underbrace{-\alpha \tanh(\kappa h(t - \tau))}_{\text{Delay term}} + \underbrace{\beta \cos(2\pi\omega t)}_{\text{Seasonal forcing}} \quad (21)$$

3.2 Stability Analysis of Eq. 19

Here we consider the stability of Suarez and Schopf's simplistic DDE in eq. 19. Based on the assumptions that the delayed wave dampens the current ENSO phase, we assume $\alpha > 0$, and based

on the expectation that the delayed wave has lost some information via dissipation in transit and imperfect reflections, we assume $\|\alpha\| < 1$.

First, we calculate the steady states by following the equilibrium definition in eq. 7.

$$\begin{aligned} 0 &= T - T^3 - \alpha T \\ 0 &= T(1 - T^2 - \alpha) \end{aligned}$$

We notice that this implies $T = 0$ or that $T^2 = 1 - \alpha$. Thus, we can conclude that

$$T = 0, \pm\sqrt{1 - \alpha}$$

are the steady states of our system.

Let's assume $T \neq 0$. Next we represent perturbations as $T(t) = T_0 + T'(t)$, and substitute:

$$\begin{aligned} \dot{T}'(t) &= (T_0 + T') - (T_0 + T')^3 - \alpha(T_0 + T')(t - \tau) \\ &= T_0 + T' - T_0^3 - 3T_0^2T' - 3T_0T'^2 - T'^3 - \alpha T_0(t - \tau) - \alpha T'(t - \tau) \\ &\approx (T_0 - T_0^3 - \alpha T_0(t - \tau)) + T' - 3T_0^2T' - (3T_0T'^2 - T'^3) - \alpha T'(t - \tau). \end{aligned}$$

Now, recalling that T_0 is a steady state of the DDE, we can collapse the collected terms down into just a function of T' :

$$\begin{aligned} &\approx 0 + T' - 3T_0^2T' - 0 - \alpha T'(t - \tau) \\ &= T'(1 - 3T_0^2) - \alpha T'(t - \tau) \\ &= T'(1 - 3(1 - \alpha)) - \alpha T'(t - \tau) \\ &= (3\alpha - 2)T' - \alpha T'(t - \tau). \end{aligned}$$

At this point, we also assume that the first coefficient is greater than the second, and therefore

$$3\alpha - 2 > -\alpha \implies 4\alpha > 2 \implies \alpha > \frac{1}{2}.$$

Thus, this restricts us to $\alpha \in (\frac{1}{2}, 1)$.

Now, as before in the zero dimensional stability analysis, let us assume a solution for the perturbation of the form $T'(t) = Te^{\sigma t}$, and substitute. We first seek neutral stability curves, where if $\sigma = \sigma_r + i\sigma_i$, then $\sigma_r = 0$.

$$\begin{aligned} Te^{\sigma t} \cdot \sigma &= (3\alpha - 2)Te^{\sigma t} - \alpha Te^{\sigma(t-\tau)} \\ \sigma &= (3\alpha - 2) - \alpha e^{-\sigma\tau}. \end{aligned}$$

Using our assumption that $\sigma_r = 0$ so that $\sigma = i\sigma_i$, we have that

$$\begin{aligned} i\sigma_i &= (3\alpha - 2) - \alpha e^{-i\sigma_i\tau} \\ i\sigma_i &= (3\alpha - 2) - \alpha(\cos(\sigma_i\tau) - i\sin(\sigma_i\tau)). \end{aligned}$$

First, matching the coefficients of the real part gives

$$\begin{aligned} 0 &= 3\alpha - 2 - \alpha \cos(\sigma_i\tau) \\ \cos(\sigma_i\tau) &= \frac{3\alpha - 2}{\alpha} \implies \tau = \frac{\arccos \frac{3\alpha - 2}{\alpha}}{\sigma_i} \end{aligned}$$



Figure 6: Neutral Stability Curve for eq. 19 with $\tau \in (0, 10)$ on the x axis, $\alpha \in (0.5, 1)$ on the y axis.

Matching the imaginary coefficients takes some more work.

$$i\sigma_i = \alpha i \sin(\sigma_i \tau)$$

$$\sin(\sigma_i \tau) = \frac{\sigma_i}{\alpha}$$

Using the identity that $\sin^2(x) + \cos^2(x) = 1$ for all $x \in \mathbb{R}$, we can combine the expression we have for $\sin(\sigma_i \tau)$ and the above formula we found for $\cos(\sigma_i \tau)$ to write that

$$\begin{aligned} \sin^2(\sigma_i \tau) + \cos^2(\sigma_i \tau) &= 1 \\ \left(\frac{\sigma_i}{\alpha}\right)^2 + \left(\frac{3\alpha - 2}{\alpha}\right)^2 &= 1 \\ \sigma_i^2 + (3\alpha - 2)^2 &= \alpha^2 \\ \sigma_i^2 &= \alpha^2 - (3\alpha - 2)^2 \\ \sigma_i &= \sqrt{\alpha^2 - (3\alpha - 2)^2} \end{aligned}$$

So, the neutral stability curve is:

$$\tau = \frac{\arccos\left(\frac{3\alpha - 2}{\alpha}\right)}{\sqrt{\alpha^2 - (3\alpha - 2)^2}}$$

The neutral stability curve is plotted in fig. 6. It is not difficult to see that cases starting below this curve are stable while cases starting above this curve are unstable.

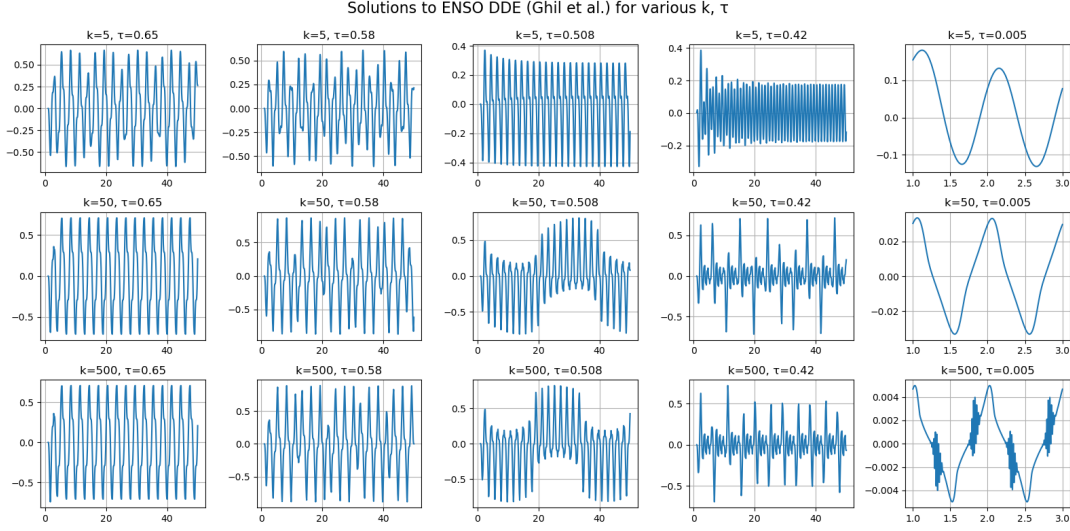


Figure 7: Solutions to eq. 22 for various κ, τ

3.3 Numerical Analysis of Eq. 21

Here we consider numerical solutions of Ghil et al.'s DDE with seasonal forcing 21.

We begin by rescaling $h(t)$, thus letting $\alpha, \beta, \omega = 1$. To solve $h(t)$ for $t > 0$, we must be able to define $h(t - \tau)$. Therefore, we must prescribe some initial state $h(t) = \phi(t)$ for $t \in [-\tau, 0]$. Here we set $\phi(t) := 1$. These choices transform our equation to:

$$\begin{cases} \dot{h}(t) = -\tanh(\kappa h(t - \tau)) + \cos(2\pi t) & \text{for } t \geq 0 \\ h(t) = 1 & \text{for } t \in [-\tau, 0] \end{cases} \quad (22)$$

We select the parameter values $\kappa = 5, 50, 500$ and $\tau = 0.65, 0.58, 0.508, 0.42, 0.005$, which model several different real-world phenomena. (Note that axes are scaled differently, for readability and comparison of shapes.)

- $\kappa \geq 50, \tau = 0.65$ represent no anomalies.
- $\kappa = 5, \tau = 0.65$ represents regular El Niño and La Niña phases.
- $\tau = 0.58$ represent anomalies in La Niña; especially for $\kappa = 500$, these are irregularly timed.
- $\kappa \geq 50, \tau = 0.508$ represent long-term variability in addition to short-term phases.
- $\kappa \geq 50, \tau = 0.42$ are arguably closest to what we experience: irregular pulses of El Niño and La Niña phases
- $\kappa = 500, \tau = 0.005$ represent bursts of intra-seasonal activity, potentially Madden-Julian oscillations.

4 Concluding thoughts

In this report, we explored the stability of steady states of DDEs in climate modeling, in particular general temperature systems influenced by delayed albedo effects and systems capturing the dynamics of the El Niño Southern Oscillation (ENSO). We described a perturbation-based framework for analyzing the stability of steady states and through basic algebra are able to uncover unique behaviors that we emphasize visually.

DDEs are exciting because they expand the expressiveness of climate models while not significantly increasing the complexity of the calculations or theoretical analysis. Despite the simplicity of adding time delays, it is clear that nontrivial and intricate dynamics emerge because of delayed feedback loops, such as the delayed albedo effect introducing bifurcations and chaotic dynamics into the global temperature model. DDE-based approaches will likely prove invaluable for capturing a greater portion of empirical climate observations and deeply understanding the complicated dynamics underlying climate change and phenomenon.

References

- [1] L. S. ANDERSSON AND P. A. LUNDBERG, *Delayed albedo effects in a zero-dimensional climate model*, Journal of Atmospheric Sciences, 45 (1988), pp. 2294–2305.
- [2] J. BJERKNES, *Atmospheric teleconnections from the equatorial pacific*, Monthly Weather Review, American Meteorological Society, 97 (1969), pp. 163–172.
- [3] M. GHIL ET AL., *A delay differential model of enso variability: parametric instability and the distribution of extremes*, Nonlinear Processes in Geophysics, 15 (2008), pp. 417–433.
- [4] N. D. HAYES, *Roots of the transcendental equation associated with a certain difference-differential equation*, Journal of the London Mathematical Society, s1-25 (1950), pp. 226–232.
- [5] A. KEANE, B. KRAUSKOPF, AND C. POSTLETHWAITE, *Climate models with delay differential equations*, Chaos: An Interdisciplinary Journal of Nonlinear Science, 27 (2017), p. 114309.
- [6] M. J. SUAREZ AND P. S. SCHOPF, *A delayed action oscillator for enso*, Journal of the Atmospheric Sciences, American Meteorological Society, 45 (1988), pp. 3283–3287.
- [7] E. TZIPERMAN ET AL., *El niño chaos: Overlapping of resonances between the seasonal cycle and the pacific ocean-atmosphere oscillator*, Science, 264 (1994), pp. 72–74.